Enhanced piezoelectric properties of (110)-oriented PbZr$_{1-x}$Ti$_x$O$_3$ epitaxial thin films on silicon substrates at shifted morphotropic phase boundary

X. Wan,[1,2] E. P. Houwman,[1] R. Steenwelle,[1] R. van Schaijk,[2] M. D. Nguyen,[1,3] M. Dekkers,[1,3] and G. Rijnders[1,a)]

[1]*MESA+ Institute for Nanotechnology, Faculty of Science and Technology, University of Twente, P.O. Box 217, 7500 AE Enschede, The Netherlands*
[2]*Holst Centre (IMEC-NL), High Tech Campus 31, 5656 AE Eindhoven, The Netherlands*
[3]*Solmates B.V., Drienerlolaan 5, 7522 NB Enschede, The Netherlands*

Piezoelectrical, ferroelectrical, and structural properties of epitaxial pseudocubic (110)$_{pc}$ oriented 500 nm thick PbZr$_{1-x}$Ti$_x$O$_3$ thin films, prepared by pulsed laser deposition on (001) silicon substrates, were measured as a function of composition. The dependence of the measurement data on the Ti content is explained by an abrupt transition from the rhombohedral r-phase to the tetragonal $(c/a)_{45}$ phase for $x \approx 0.6$, indicating a shift of the Morphotropic Phase Boundary to this value, where the effective piezoelectric coefficient $e_{31,eff}$ and dielectric constant $\varepsilon_{33,eff}$ reach their maximum values. These findings are of great significance for Si-based piezo-micro electro mechanical systems, in particular energy harvesters. The largest value of the figure-of-merit for such devices was found for $x = 0.6$, $FOM = 24.0 \, GPa$. © 2014 AIP Publishing LLC. [http://dx.doi.org/10.1063/1.4867477]

Piezoelectric (PE) thin films based on lead zirconate titanate (PZT) material have been attracting significant interest in view of their applications in piezo-microelectromechanical systems (MEMS).[1–3] One of such applications is in Piezo-MEMS micro scale energy harvesters that convert vibrational energy into electrical energy,[4–6] which potentially offers an ideal way to generate and store power for self-powered wireless sensor systems. A critical performance benchmark for such an energy harvester device is the figure of merit ($FOM = e_{31,eff}^2 / \epsilon_0 \epsilon_{33,eff}$), which is directly proportional to its power output.[7,8] Here, $e_{31,eff}$ is the relevant effective piezoelectric coefficient and $\varepsilon_{33,eff}$ is the dielectric constant. Effective parameters of the thin film device are defined with respect to the axes system of the thin-film (index 1 and 2 for the in plane directions, 3 for the out of plane direction), which may differ from the single crystal values which are defined with respect to the (pseudocubic) crystal axes. Energy harvesters need to operate for a large number of cycles, therefore, a deposition process is required that produces reliable devices, which do not show significant degradation of properties. Si is the substrate material of choice for MEMS devices. Therefore, there is a strong research effort to integrate PZT thin film technology with Si substrates.[9,10] Pulsed laser deposition (PLD) is such a technique. Depending on the buffer layer one can grow (001)$_{pc}$, (111)$_{pc}$, or (110)$_{pc}$ oriented epitaxial films by PLD on Si(001) substrates. (We will use the pseudocubic lattice system for designating planes and directions in the PZT film.) The properties of epitaxial (001)$_{pc}$ and (111)$_{pc}$ PZT thin films on Si(001) deposited by other CVD techniques have been reported in literature.[11] Here, we report on the piezoelectric and ferroelectric (FE) properties of (110)$_{pc}$ films on Si as a function of the Ti-fraction x in the PbZr$_{1-x}$Ti$_x$O$_3$ in relation to the crystalline structure. A thorough understanding of this relation is essential for optimizing the material properties of piezo material thin films in Piezo MEMS devices.

Epitaxial PZT thin films, deposited at high temperature (600 °C) and cooled down to room temperature, show residual stress depending on the choice of the substrate, due to the difference in thermal expansion coefficients, causing differences in FE and PE properties.[9,12,13] These effects have extensively been modeled by Pertsev *et al.*[14] and Kukhar *et al.*[15] for thick, (001)$_{pc}$ oriented, clamped films. The thermal stress in thick films at the tetragonal side of the phase diagram (at large Ti-content) can be relaxed by c/a domain formation (domains of tetragonal unit cells with the long axis perpendicular, respectively, parallel to the film plane) and the FE/PE properties are largely determined by the change in the c-domain fraction, ϕ_c, under influence of an external stress or electrical field. Only for very large strains, the crystallographic structure changes either to a c-domain phase (large compressive strain) or a_1/a_2 domain phase (large tensile strain, with only tetragonal domains laying in-plane). However, if the composition is near the bulk crystal Morphotropic Phase Boundary (MPB) (at Ti-content $x = 0.48$) between the bulk crystal rhombohedral and tetragonal phase an additional r-phase (or r_1/r_2-phase in a multidomain structure) appears over a wide range of misfit strain in which the polarization can easily rotate in the {110}$_{pc}$ planes perpendicular to the substrate under the influence of an external applied strain or electrical field. Due to this easy rotation, the dielectric and PE properties are generally much larger in this phase, and diverge at the boundary of this phase with the c/a phase. We show that these features also apply qualitatively to the investigated (110)$_{pc}$-oriented PZT films on Si, resulting in a very large FOM at the phase boundary. This phase boundary is at $x \approx 0.6$, which is different from the MPB value in a bulk, randomly oriented polycrystalline ceramic.

PLD was used to deposit the 100 nm SrRuO$_3$ (SRO) bottom electrode layer, the 500 nm (110)$_{pc}$-oriented PbZr$_{1-x}$Ti$_x$O$_3$ piezoelectric layer, and 100 nm Pt top electrode of the capacitor. The Ti-fraction was $x = 0.8, 0.7, 0.6, 0.55,$

---

a)Author to whom correspondence should be addressed. Electronic mail: a.j.h.m.rijnders@utwente.nl

0.48, and 0.4. For the $e_{31,eff}$ bending tests, the capacitors have dimensions 2×8 mm^2 on a 500 μm thick 3×25 mm^2 Si-strip. The sandwich capacitor structures were epitaxially grown on a 50 nm Yttria-Stabilized Zirconia (YSZ) buffer layer deposited on the native oxide layer of Si (001) substrates. The first few nm is deposited in an Ar-plasma, so that the YSZ scavenges the Si-oxide layer.[9,16] Crystalline properties were characterized by high-resolution X-Ray Diffraction (XRD, with a PANalytical X-pert system and Bruker D8). The polarization hysteresis (PE) loops were measured in an aixACCT Analyzer TF 2000. From the loops, the remanent polarization P_r, and the spontaneous polarization P_s were determined. The transverse piezoelectric coefficient $e_{31,eff}$ was obtained by a 4-point bending measurement setup (aix4PB) in combination with the TF analyzer, at 1 Hz and zero bias field.[17] The dielectric constant $\varepsilon_{33,eff}$ at zero applied electric field was obtained from capacitance-voltage (CV) measurements at 10 kHz (Süss MicroTech PM300 probe station from SÜSS MicroTec Test Systems GmbH, equipped with a Keithley 4200 Semiconductor characterization system). A separate set of bimorph cantilever devices (also with SRO electrodes; length of 400 μm, width of 100 μm, Si beam thickness of 5 μm) was made using a 675 μm thick Silicon-On-Insulator (SOI) wafer with a 5 μm device layer and a 0.5 μm Buried OXide (BOX) layer. From the dynamic deflection under applied voltage, the effective piezoelectric coefficient $d_{31,eff}$ of the material was determined (Polytec Laser Doppler Vibrometer (LDV)) using the procedure described in Ref. 18 and the PZT elastic property data in Ref. 14.

The crystalline properties of PbZr$_x$Ti$_{1-x}$O$_3$ thin films were determined from θ-2θ XRD patterns, as shown in Fig. 1. It is concluded that all films are epitaxially grown on the silicon with (110)$_{pc}$ orientation. Fig. 1(b) shows that for $x = 0.4 - 0.6$ there is a single reflection with the same narrow FWHM of approximately 0.2°. The peak shift reflects the change of the out-of-plane lattice parameter with x. There is an abrupt change in the reflections for the films with $x > 0.6$. The FWHM approximately doubles and a second reflection appears, corresponding to a second, smaller out-of-plane lattice parameter. At the tetragonal side of the PZT phase diagram, one expects crystallographic domains with the c-axis in the film plane ("a_{45}-domains") with the a-axis under 45° angle with the film surface and analogously defined c_{45}-domains, explaining the appearance of two out-of-plane lattice parameters. (We use the subindex 45 to distinguish this domain type in (110)$_{pc}$ films from the a and c-domains in (001)$_{pc}$ films.) For $x = 0.4 - 0.6$ films, the XRD shows that the pseudocubes have a single out-of-plane lattice parameter throughout the film, which is an indication for the r-phase.

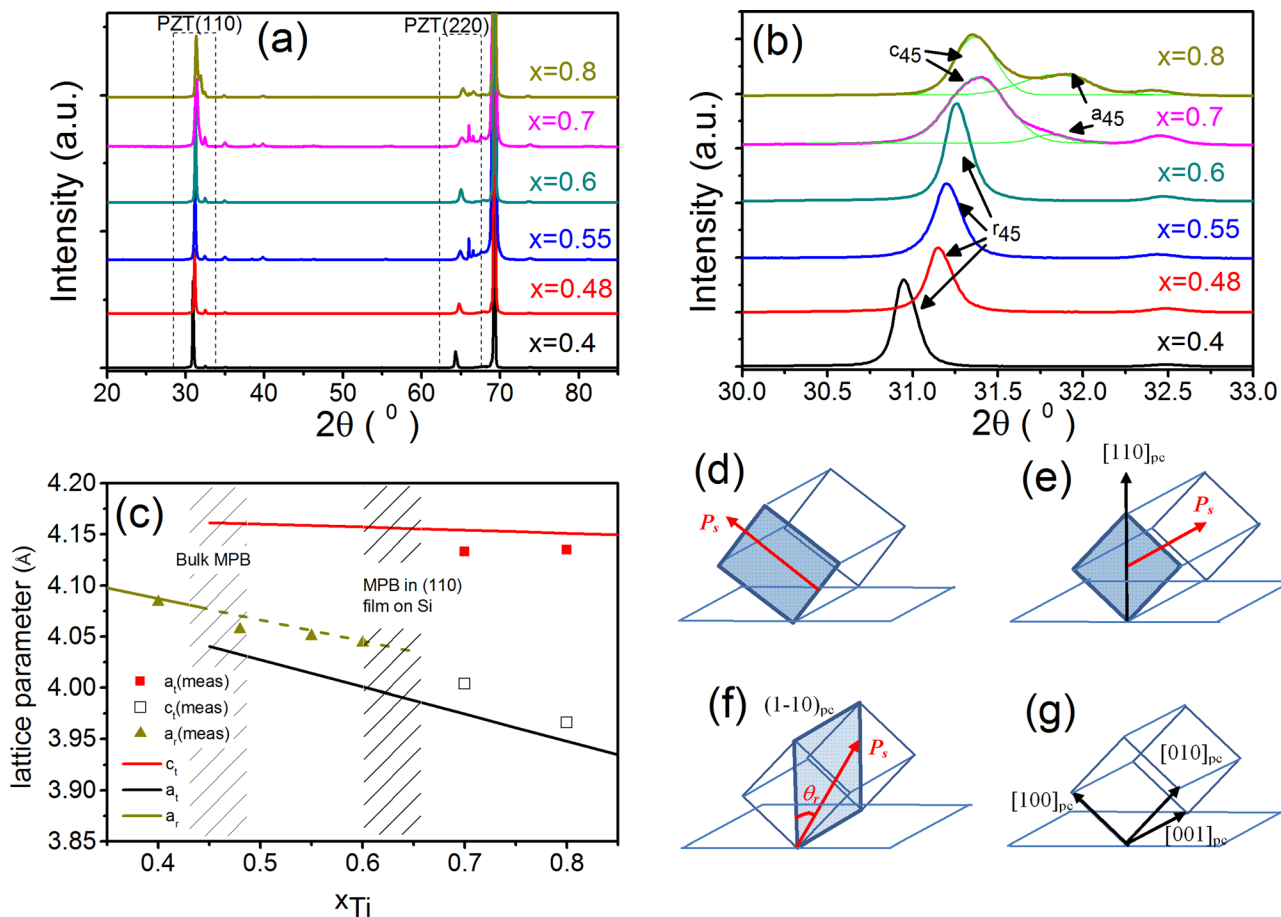From detailed XRD reciprocal space maps, the in-plane and out-of-plane lattice parameters were obtained. For

FIG. 1. XRD pattern of PbZr$_{1-x}$Ti$_x$O$_3$ (110)$_{pc}$ thin films on silicon substrates. (a) Full scan; (b) zoom in around (110)$_{pc}$ peak, showing two out-of-plane lattice parameters for $x > 0.6$; (c) lattice parameters for thick (110)$_{pc}$ films. Tilted tetragonal unit cell: (d) c_{45}-domain (shaded $a \times c$ (001)$_{pc}$ plane; (e) a_{45}-domain with shaded $a \times a$ (001)$_{pc}$ plane. (f) Tilted rhombohedral unit cell: shaded $(1\bar{1}0)_{pc}$ plane, in which the polarization vector rotates over the angle θ_r. (g) Pseudocubic unit cell lattice vectors of a (110)$_{pc}$ film.

$x \leq 0.6$, the XRD-data can best be fitted with a (rhombohedral) PZT-pseudocube. In the range $x \geq 0.7$, two tilted tetragonal pseudocubes can be identified. The lattice parameters are plotted in Fig. 1(c). The transition from the $(c/a)_{45}$-phase to r_1/r_2-phase at $x \approx 0.6 - 0.66$ for these thick $(110)_{pc}$ films is indicated by the shaded region. Also are shown the lines corresponding to the lattice parameters of bulk (stress free) PZT as a function of composition (obtained from the model of Ref. 19 which describes the experimental bulk data very well). The line corresponding to the rhombohedral lattice parameter a_r has tentatively been extended to higher Ti-fraction. It is observed that the measured a_r follows this line well up to the phase transition. The experimental data of $x = 0.8$, 0.7 for the $(110)_{pc}$-films slightly deviate from the model lines, which may indicate the presence of some strain in these unit cells.

In Fig. 2, we plotted the average strain S_m, (defined analogously to the definition used by Kukhar *et al.*[15]) calculated for the tetragonal $(110)_{pc}$-films as a function of the c_{45}-domain fraction[20] using the measured (tetragonal) lattice parameters. The underlying model assumes that all strain is relaxed by adapting the domain fraction, such that the stress in the unit cells is fully relaxed. S_m is a linear function of the domain fraction ϕ_{c45} of c_{45} domains. The calculated S_m should be equal to the average strain imposed by the substrate, $S_{m,cl} = \left(a_s^*(T) - a_c(T)\right)/a_c(T)$, where $a_s^*(T) = a_s^*(T_d)$ $[1 - \alpha_s \Delta T]$ is the effective substrate lattice parameter at room temperature T. This can be achieved by adapting the domain fraction accordingly. $S_{m,cl}$ is obtained from the measured relaxed film (cubic) lattice parameter at deposition temperature T_d and the Si substrate thermal expansion coefficient α_s. $\Delta T = T_d - T$ and $a_c(T)$ are the film pseudocubic lattice parameter. $S_{m,cl}$ was calculated and plotted in Fig. 2 for the measured domain fraction of the corresponding film. $S_{m,cl}$ and S_m are equal within less than 0.1% strain. This correspondence is considered to be good, considering the inaccuracies in the measured data. A further reason for the small discrepancies may be that the model assumes full stress relaxation in the unit cell and that all thermal stress in the film is resolved by shifting the domain fraction. However,
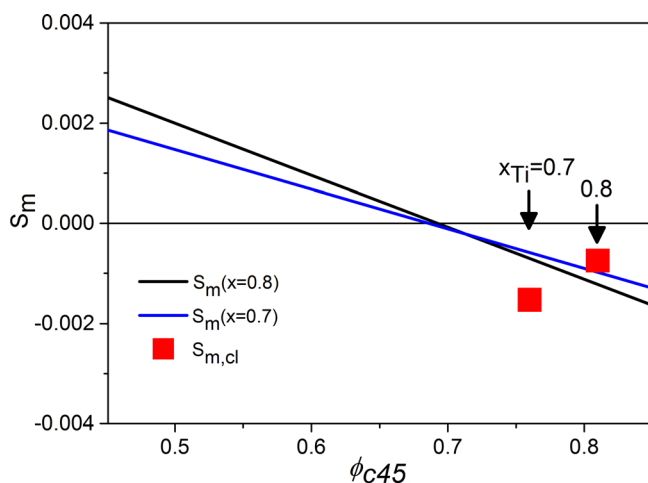
Fig. 1(c) indicates that the tetragonal unit cells are slightly strained. This changes also the polarization of the unit cell and thus the domain fraction. The slightly reduced c-axis length would correspond to a somewhat smaller P_s of the unit cell, hence to a slightly larger domain fraction $P_s(meas)/(P_s/\sqrt{2}) = \phi_{c45,s}$. The $(110)_{pc}$ PZT thin film can relax stress in several ways. Near the deposition temperature this occurs through misfit dislocations (grain boundaries, threading dislocations), but at lower temperatures linear strain and/or angular distortion of the pseudocube may build up, and below the transition temperature strain can also be relaxed by crystallographic domain configurations. The resulting strain is due to minimization of the free energy with respect to polarization domain structure and linear and angular strain. The XRD data indicate that the angular distortion of the rhombohedral phase is the energetically most favorable way to relax the strain for $x \leq 0.6$, whereas for the more tetragonal compositions it is by $(c/a)_{45}$ domain formation.

In the following, we show that the phase change is reflected in a divergence of the dielectric, ferroelectric, and piezoelectric properties at the r-$(c/a)_{45}$ phase boundary, similarly as predicted by the model for $(001)_{pc}$ films.

Polarization hysteresis loops were measured after 10^8 cycles. After an initial poling procedure no degradation of the loops is observed up to this number of cycles, proving the stability of these devices. In Fig. 3, the spontaneous polarization $P_s(meas)$, determined from the P-axis cutoff of the high-field tangent to the loops, is given, as well as the literature values P_s for the spontaneous polarization.[21] For the r-phase, one expects that the polarization vector can easily rotate in the $(1\bar{1}0)_{pc}$ symmetry plane of the $(110)_{pc}$ oriented pseudocube, under influence of the applied field or by strain. Thus one can write for the measured remanent polarization $P_r(meas) = P_s \cos \theta_r$, where θ_r is the angle of the polarization vector with the film normal. The curve $P_r(meas)$ is drawn for

FIG. 2. Calculated average strain S_m in (110) oriented PZT films with $x_{Ti} = 0.7$ and 0.8 as a function of the c_{45} domain fraction ϕ_{c45}. The data points are average strain values, determined from the thermal mismatch of the substrate with the film.
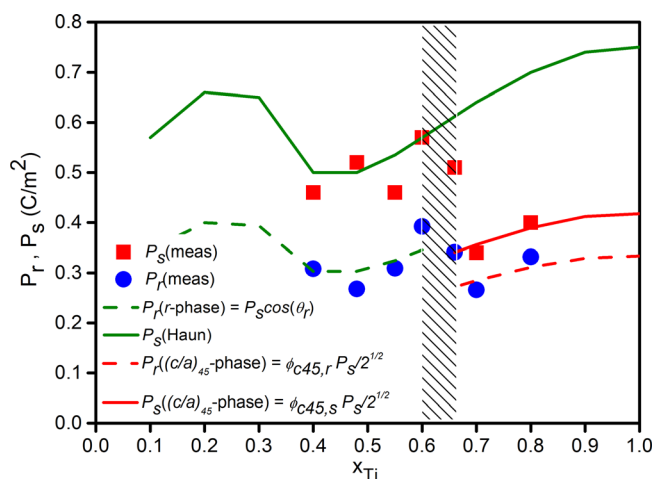

FIG. 3. Spontaneous and remanent polarization of $(110)_{pc}$-oriented PbZr$_{1-x}$Ti$_x$O$_3$ thin films (500 nm). The curve P_s(Haun) indicates the bulk spontaneous polarization values according to Ref. 21. The remanent polarization P_r of the r-phase is calculated as $P_s \cos(\theta_r)$, with θ_r the (average) angle of the r-phase polarization vector with the film normal. In the $(c/a)_{45}$-phase, the P_s and P_r are determined by the fraction ϕ_{c45} of tetragonal domains with out of plane polarization $P_s/\sqrt{2}$. The shaded area indicates the transition between the r-phase and the tetragonal $(c/a)_{45}$-phase. The data points are obtained from bending test samples.

a tilt $\theta_r = 53°$, which is the average for the four r-phase compositions. Note that the polarization vector in this case is rotated much further into the plane then if it were aligned along the body diagonal ($\theta_r = 35°$), indicating a significant shear deformation in the $(1\bar{1}0)_{pc}$ plane as well. For large fields, the polarization is aligned along the field direction and $P_s(meas) = P_s$. In the tetragonally distorted pseudocubic $(c/a)_{45}$ phase, the spontaneous polarization is determined by the domain fraction ($\phi_{c45,s}$) of c_{45} domains, $P_s(meas) = \phi_{c45,s}P_s/\sqrt{2}$. The domain fraction cannot easily be changed by the electrical field, since this involves a large change in the elastic energy of the system. Therefore, the domain fraction at zero field, $\phi_{c45,r}$, determining the remanent polarization, is only slightly smaller. This behavior is clearly observed in Fig. 3: for $x \leq 0.6$ the measured P_s and P_r are well described by the literature value $P_s(x)$ and $P_s(x)cos\theta_r$, whereas at $x > 0.66$ there is an abrupt jump in P_s and secondly P_s and P_r differ much less. The domain fractions are approximately $\phi_{c45,s} \approx 0.79$ and $\phi_{c45,r} \approx 0.63$, indicating that approximately 16% of the domains change orientation under high field conditions. The case of $x = 0.66$ shows polarization values intermediate between the r-phase and $(c/a)_{45}$-phase.

The measured values of the effective piezoelectric parameter $e_{31,eff} = dD_3/dS_1$, and the dielectric parameter $\varepsilon_{33,eff}$ are shown in Fig. 4. The $e_{31,eff}$ measurements have been repeated for two other sets of devices, prepared in separate deposition runs, to confirm the reproducibility. Also are shown the $\varepsilon_{33,eff}$ of the same films and with these data, the *FOM* values were calculated (Fig. 4), showing an extreme value of 24 GPa for $x = 0.6$. Further, the $d_{31,eff}$ values of the $(110)_{pc}$ cantilever films are shown. The bending test samples show a sharp increase of $e_{31,eff}$ and $\varepsilon_{33,eff}$ at the r-phase side of the phase diagram going towards the phase boundary, as is also predicted for $\varepsilon_{33,eff}$ by the model for $(001)_{pc}$ films.[15] This model also indicates that the properties only change gradually at the c/a side of the phase. The transition is found for the same Ti-fraction as found in the
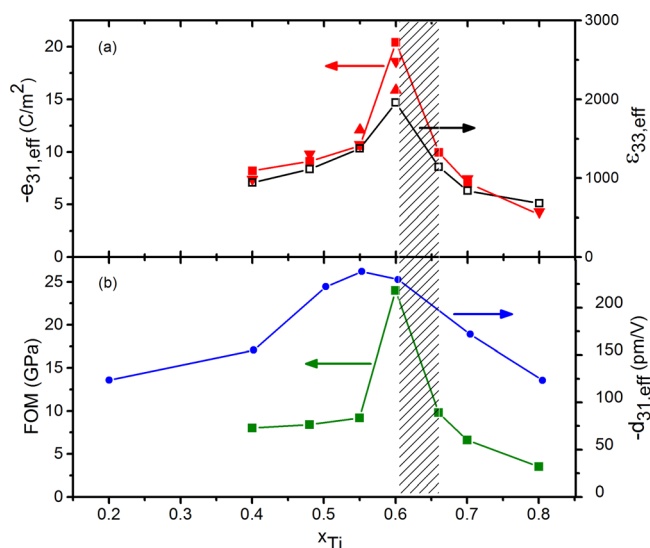
structural and polarization data of the $(110)_{pc}$-films. The $d_{31,eff}$ data of the cantilever films show a broader peak, at approximately the same Ti-content as for the bending test films. The difference in peak width between the samples is ascribed to the differences in the thickness of the substrate (500 μm versus 5 μm for bending test samples and cantilever samples, respectively) and the measurement methods (static under a slight tensile preload versus dynamic at zero preload).

In conclusion, PbZr$_{1-x}$Ti$_x$O$_3$ thin films with $(110)_{pc}$ orientation were grown on silicon substrates with $x = 0.4 - 0.8$. The crystallographic and FE/PE data are consistent with the model that the ferroelectric domains are in the rhombohedral r-phase for $x \leq 0.6$ and in the tetragonal multidomain $(c/a)_{45}$ phase for $x > 0.6$. At the r-side of the phase diagram close to the phase boundary, these films show very large piezoelectric and dielectric properties. From bending tests on samples on thick Si substrates a maximum $e_{31,eff}$ value of 20.4 C/m^2 is achieved at the r-$(c/a)_{45}$ phase boundary, resulting in a $FOM = 24$ GPa. The same qualitative behavior is found in $d_{31,eff}$ data of films on thin Si cantilevers. The shift of the peak in the properties from the Morphotropic Phase Boundary at $x = 0.48$ in bulk PZT towards the Ti-rich side in the phase diagram is ascribed to the clamping of the film on Si in combination with the $(110)_{pc}$ orientation of the film. This shift can be understood in the framework of the model of Kukhar *et al.*, describing the broadening of the r-phase at the MPB. The very large FOM of the PZT thin film with near $(c/a)_{45}$-r phase boundary composition is of great significance for the development and implantation in piezo-micro electromechanical devices like energy harvesters.

FIG. 4. (a) Piezoelectric coefficient $e_{31,eff}$, dielectric constant $\varepsilon_{33,eff}$ and (b) FOM determined from bending beam devices; piezoelectric coefficient $d_{31,eff}$ determined from cantilever devices as function of composition in $(110)_{pc}$-oriented PbZr$_{1-x}$Ti$_x$O$_3$ thin films.

[1]P. Muralt, J. Am. Ceram. Soc. **91**, 1385 (2008).

[2]S. H. Baek, J. Park, D. M. Kim, V. A. Aksyuk, R. R. Das, S. D. Bu, D. A. Felker, J. Lettieri, V. Vaithyanathan, S. S. Bharadwaja, N. Bassiri-Gharb, Y. B. Chen, H. P. Sun, C. M. Folkman, H. W. Jang, D. J. Kreft, S. K. Streiffer, R. Ramesh, X. Q. Pan, S. Trolier-McKinstry, D. G. Schlom, M. S. Rzchowski, R. H. Blick, and C. B. Eom, Science **334**, 958 (2011).

[3]S. Trolier-McKinstry and P. Muralt, J. Electroceram. **12**, 7 (2004).

[4]P. Muralt, R. G. Polcawich, and S. Trolier-Mckinstry, MRS Bull. **34**, 658 (2009).

[5]D. Isarakorn, D. Briand, P. Janphuang, A. Sambri, S. Gariglio, J. M. Triscone, F. Guy, J. W. Reiner, C. H. Ahn, and N. F. de Rooij, Smart Mater. Struct. **20**, 025015 (2011).

[6]R. J. M. Vullers, R. van Schaijk, I. Doms, C. Van Hoof, and R. Mertens, Solid-State Electron. **53**, 684 (2009).

[7]J. E. A. Southin, S. A. Wilson, D. Schmitt, and R. W. Whatmore, J. Phys. D: Appl. Phys. **34**, 1456 (2001).

[8]K. Karakaya, M. Renaud, M. Goedbloed, and R. Van Schaijk, J. Micromech. Microeng. **18**, 104012 (2008).

[9]M. Dekkers, M. D. Nguyen, R. Steenwelle, P. M. te Riele, D. H. A. Blank, and G. Rijnders, Appl. Phys. Lett. **95**, 012902 (2009).

[10]F. Calame and P. Muralt, Appl. Phys. Lett. **90**, 062907 (2007).

[11]S. Yokoyama, Y. Honda, H. Morioka, T. Oikawa, H. Funakubo, T. Iijima, H. Matsuda, and K. Saito, Appl. Phys. Lett. **83**, 2408 (2003).

[12]M. P. Warusawithana, C. Cen, C. R. Sleasman, J. C. Woicik, Y. Li, L. F. Koukoutis, J. A. Klug, H. Li, P. Ryan, L. Wang, M. Bedzyk, D. A. Muller, L. Q. Chen, J. Levy, and D. G. Schlom, Science **324**, 367 (2009).

[13]A. K. Sharma, J. Narayan, C. Jin, A. Kvit, S. Chattopadhyay, and C. Lee, Appl. Phys. Lett. **76**, 1458 (2000).

[14]N. Pertsev, V. Kukhar, H. Kohlstedt, and R. Waser, Phys. Rev. B **67**, 054107 (2003).

[15]V. Kukhar, N. Pertsev, H. Kohlstedt, and R. Waser, Phys. Rev. B **73**, 214103 (2006).

[16]M. D. Nguyen, R. J. A. Steenwelle, P. M. te Riele, J. M. Dekkers, D. H. A. Blank, and C. Rijnders, in *Proceedings of the 22nd International conference on EUROSENSORS* (Dresden, Germany, 2008), p. 810.

[17]K. Prume, P. Muralt, F. Calame, T. Schmitz-Kempen, and S. Tiedke, J. Electroceram. **19**, 407 (2007).

[18]M. Dekkers, H. Boschker, M. van Zalk, M. D. Nguyen, H. Nazeer, E. Houwman, and G. Rijnders, J. Micromech. Microeng. **23**, 025008 (2013)

[19]G. A. Rossetti, A. G. Khachaturyan, G. Akcay, and Y. Ni, J. Appl. Phys. **103**, 114113 (2008).

[20]In general, the misfit strain is defined as $S_m = (a - a_{pc})/a_{pc}$ with a the strained lattice constant and a_{pc} the pseudocubic lattice constant. For the considered $(110)_{pc}$ films, we neglect the $10°$ misalignment of the pseudocubes with the $Si\langle 001\rangle$ axes and the small tilt of the pseudocubes with respect to the film normal, so that for the $(c/a)_{45}$ domain structure the in-plane axes are $b = \sqrt{a^2 + c^2}$, respectively, a for the c_{45} domains, resulting in the strains $S_{c1} = \left(b - a_{pc}\sqrt{2}\right)/a_{pc}\sqrt{2}$ and $S_{c2} = (a - a_{pc})/a_{pc}$ each with fraction $\phi_{c45}/2$ and $a_{\sqrt{2}}$, respectively, c for the a_{45}-domains with strains $S_{a1} = (a - a_{pc})/a_{pc}$ and $S_{a2} = (c - a_{pc})/a_{pc}$, each with fraction $(1-\phi_{c45})/2$. The fraction weighted average misfit strain is then $S_m = (\phi_{c45}/2)(S_{c1} + S_{c2}) + ((1 - \phi_{c45})/2)(S_{a1} + S_{a2})$.

[21]M. J. Haun, E. Furman, S. J. Jang, and L. E. Cross, Ferroelectrics **99**, 63 (1989).